

Deformation of convergent plates: Evidence from discrepancies between GPS velocities and rigid-plate motions

Youqing Yang and Mian Liu

Department of Geological Sciences, University of Missouri, Columbia, MO, USA.

Received 8 May 2001; revised 24 October 2001; accepted 14 November 2001; published 30 May 2002.

[1] Systematic discrepancies between the Global Positioning System (GPS) site velocities and those predicted by plate-motion models across the Andes, the Himalayan-Tibetan plateau, and the Taiwan orogen delineate diffuse plate-boundary deformation and significant intraplate deformation, even in the presumably rigid oceanic plates. The relationship between the GPS velocities and the predictions of plate-motion models is illustrated using a simple timescale-dependent mechanical model of plate convergence. A simple stiffness number (ϕ), based on the difference between the predictions of plate-motion models and the GPS velocity near plate boundaries, provides a convenient measure of the “plate-like” behavior of convergent plates and strain partitioning between intraplate and interplate deformation. *INDEX TERMS*: 8102 Tectonophysics: Continental contractional orogenic belts; 8158: Evolution of the Earth: Plate motions—present and recent (3040)

1. Introduction

[2] The basic tenet of the plate tectonics theory is that tectonic plates are rigid and crustal deformation is concentrated within narrowly defined plate boundaries. Studies in the past decades have proven this tenet to be essentially valid in most places, especially for oceanic plates. One of the most satisfying tests is the general agreement between the Global Positioning System (GPS) velocities and the prediction of rigid-plate motion models at many parts of the Earth's surface [Larson *et al.*, 1997; Stein, 1993]. However, it is well known that deformation diffuses over broad regions at some convergent plate boundaries, where the GPS velocities usually show a systematic deviation from plate-model predictions [Larson *et al.*, 1999; Leffler *et al.*, 1997]. Here we use such discrepancies across the Andes, the Himalayan-Tibetan plateau, and the Taiwan orogen to illustrate diffuse plate boundary deformation in these regions. We investigate the relationship between instantaneous and long-term averaged plate motions using a simple timescale-dependent mechanical model, and discuss strain partitioning at plate boundaries using GPS data.

2. GPS Velocities vs. Plate-Motion Model Predictions

2.1. The Andes

[3] The Andean mountain belt has resulted from subduction of the Nazca plate underneath the South America plate in the past ~ 30 Myr [Isacks, 1988]. The present-day plate convergence and the Andean crustal shortening are revealed by recent GPS measurements [Angermann *et al.*, 1999; Leffler *et al.*, 1997; Norabuena *et al.*, 1999] (Figure 1a). Between site EISL in the Nazca plate and sites in stable South America (UEPP and BRAZ) there is ~ 66 mm yr⁻¹ convergence. About half of the convergence is consumed by sliding in the subduction zone and the rest is locked

at the plate boundary, causing the coastal region to move 30–40 mm yr⁻¹ eastward with respect to stable South America [Leffler *et al.*, 1997]. The GPS velocity drops gradually over the 1000-km wide Andean orogen, indicating a crustal shortening pattern significantly different from that reflected in geological record [Liu *et al.*, 2000].

[4] The deformation of these convergent plates can be better illustrated by comparing the GPS site velocities with the predictions of plate-motion models (Figure 1b). The comparison is within the same reference frame of a fixed stable South America. For each GPS site the corresponding rigid-plate velocity was calculated from the Nuvel-1A model [DeMets *et al.*, 1994] because of the large area spanned by the GPS sites. The Nuvel-1A velocities are identical along the small circle around the Euler pole for the Nazca-South America relative motion (Figure 1a), whereas along the EISL-BRAZ profile the Nuvel-1A velocities deviate $<1\%$ from that along the small circle. So the contrasts between the GPS and Nuvel-1A velocities in Figure 1a reflect primarily the difference between active crustal deformation and the prediction of plate-motion models. The plate boundary is marked by the sharp drop of GPS velocity at the trench and diffuse deformation across the Andes. Note that at all four sites on the Nazca plate the GPS velocity is consistently lower than the Nuvel-1A predictions. Because the Nuvel-1A model was based on marine magnetic anomalies averaged over the past 3 Myr, the lower GPS velocities were explained as indications of a slowing of plate convergence [Norabuena *et al.*, 1999]. This is best shown by the ~ 14 mm yr⁻¹ difference between the Nuvel-1A and GPS velocities at EISL, a GPS site near the spreading center. However, the ~ 6 mm yr⁻¹ drop of the GPS velocity from EISL to ISFE near the trench may represent intraplate shortening of the Nazca plate, because these two sites are predicted to have almost identical eastward velocity in the Nuvel-1A model. Similar drop of GPS velocity is found at sites IRCR and GALA but with larger errors. The corresponding strain rate is up to 7×10^{-17} s⁻¹, comparable to that of some continental deformation. Although data from the Nazca plate may be too sparse to firmly delineate intraplate deformation, we show below that similar patterns of deformation are observed in other convergent plates.

2.2. The Himalayan-Tibetan Plateau

[5] The India-Eurasia collision and continued convergence in the past ~ 50 –70 Myr have led to the formation of the Himalayan-Tibetan plateau. The collisional deformation diffused thousands of kilometers into the Eurasia plate [Tapponnier and Molnar, 1979]. This is clear from recent GPS measurements (Figure 2a). For comparison we converted the GPS velocities from three groups [Chen *et al.*, 2000; Larson *et al.*, 1999; Wang *et al.*, 1999] into those relative to stable Eurasia using the No-Net-Rotation Nuvel-1A (NNR-A) absolute plate motion model [Argus and Gordon, 1991]. Note the diffuse deformation over the Tibetan plateau.

[6] Figure 2b shows that the GPS velocities at the interior India (IISC) and Eurasia (IRKT) plates are almost identical to the Nuvel-1A predictions. Between these two stations there is ~ 50 mm yr⁻¹ N-S convergence, agreeing with the Nuvel-1A model. As the sites

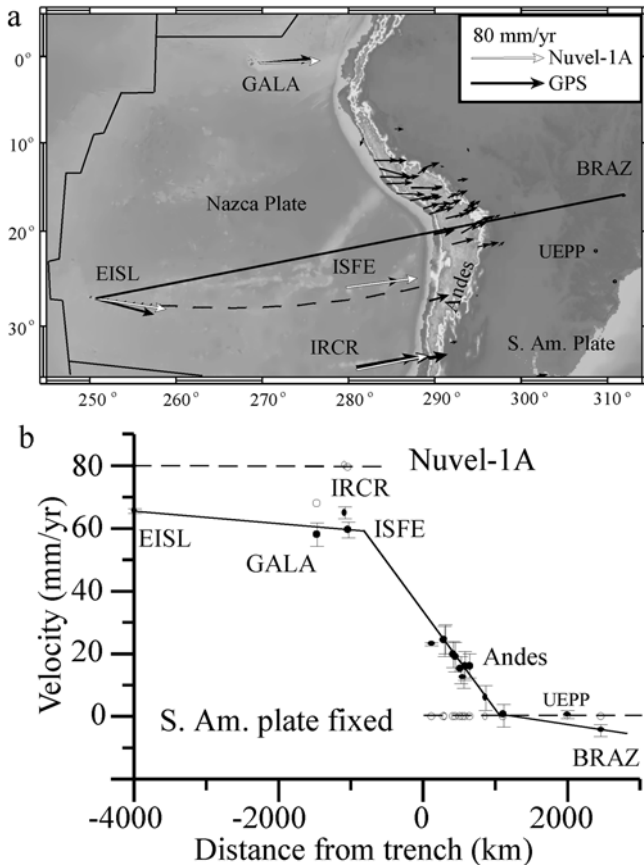


Figure 1. (a) GPS sites velocities relative to stable South America (data are from Angermann *et al.* [1999] and Norabuena *et al.* [1998]). The dashed line is a small circle through EISL around the Euler pole for the Nazca-South America relative motion. Along the circle site velocities should have the same magnitude for rigid plates. The solid line shows the location of the profile in (b). (b) Comparison of the GPS velocities (black dots with error bars) with Nuvel-1A model predictions (open circles) along the EISL-BRAZ profile. All Andean GPS sites within 200 km of the profile were projected. The dashed lines fit the Nuvel-1A velocity along the small circle in (a), and the solid line fits the GPS velocities. Only the east velocity component is shown for clarity.

approach the Main Boundary Fault (MBF), the discrepancy between the GPS and the Nuvel-1A velocities increases. Across the MBF, the GPS velocity drops from 44 mm yr^{-1} at BIRA at the northern rim of the India plate to 23 mm yr^{-1} at LHAS in southern Tibet, representing $\sim 40\%$ of the total N-S contraction between IRKT and IISC. The average strain rate is $1.7 \times 10^{-15} \text{ s}^{-1}$ across the Himalayan front. The rest of the convergence is distributed across the Tibetan plateau and a broad region in central Asia. The nearly linear GPS velocity change over the Tibetan plateau is similar to that over Central Andes (see Figure 1b). Some recent GPS measurements [Frey Mueller *et al.*, 2000] indicate a more smooth velocity drop across both the Himalayas and the Tibetan plateau than those shown in Figure 2b.

[7] Besides the broad deformation within the Eurasia plate, Figure 2b also indicates significant shortening within the India plate, the rigid indenter. Between IISC and the northern rim of the India plate (sites MAHE, NEPA, and others) there is about 4 mm yr^{-1} shortening, indicating a strain rate of $8 \times 10^{-17} \text{ s}^{-1}$. The corresponding N-S compression within the interior of the India plate are consistent with the predominately thrust-fault earthquakes

on westerly striking planes in central India [Singh *et al.*, 1999] including the 26 Jan. 2001 Gujarat earthquake.

2.3. The Taiwan Orogen

[8] The Taiwan orogen is another example of complicated plate boundary deformation. It has resulted from convergence between the Philippine Sea and the Eurasian plates during late Cenozoic. The active mountain building is shown by the recent GPS measurements [Yu *et al.*, 1997] (Figure 3). We mapped the GPS velocities onto the Eurasia-fixed reference frame by using the GPS velocity at TAIW (TAPN) [Larson *et al.*, 1999] with respect to stable Eurasia and adding this velocity vector to the rest GPS site. The area covered by the Taiwan GPS network is small (about $2^\circ \times 3^\circ$) that a uniform translation may be justified, and there is no evidence of significant rotation of the Taiwan islands with respect to stable Eurasia. Figure 3 compares the GPS velocities with the Nuvel-1A. At Lanhsu, an island on the Philippine Sea plate, the GPS velocity is almost identical to the Nuvel-1A value. However, as the sites approach the Longitude Valley Fault (LVF), the present-day plate

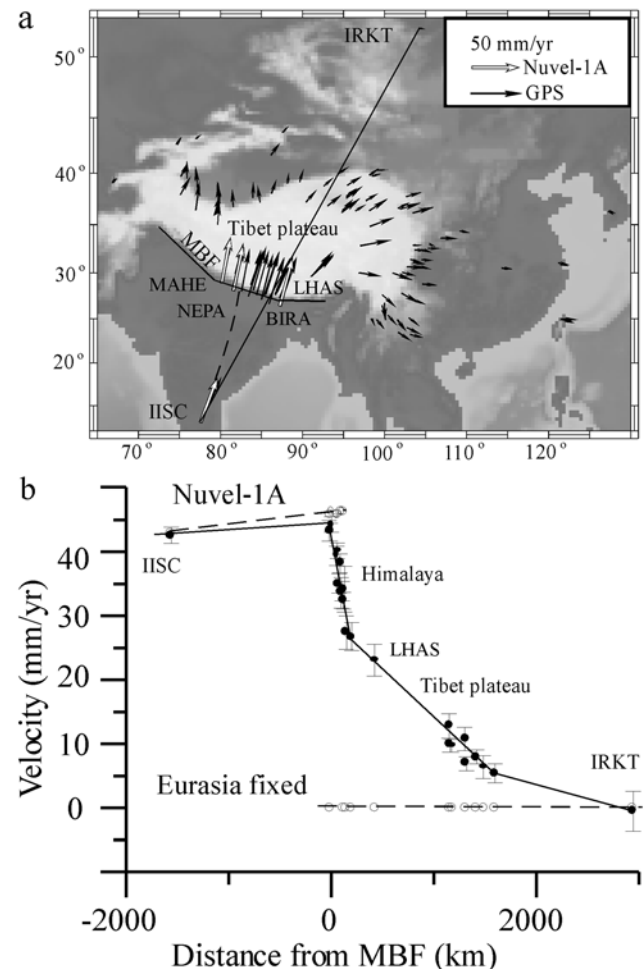


Figure 2. (a) GPS velocities across the India-Eurasia plate boundary with respect to stable Eurasia. The dashed line is a small circle around the India-Eurasia Euler pole, along the circle the Nuvel-1A velocity has the same magnitude. The solid line shows the location of the profile in (b). Nuvel-1A velocities along this profile deviate $<2\%$ from that on the small circle. (b) Comparison of the GPS site velocities (black dots with error bars) with the Nuvel-1A velocities (open circles) along a profile from IISC to IRKT. GPS sites within a 200 km swath along the profile are projected. Only the north component is shown for clarity.

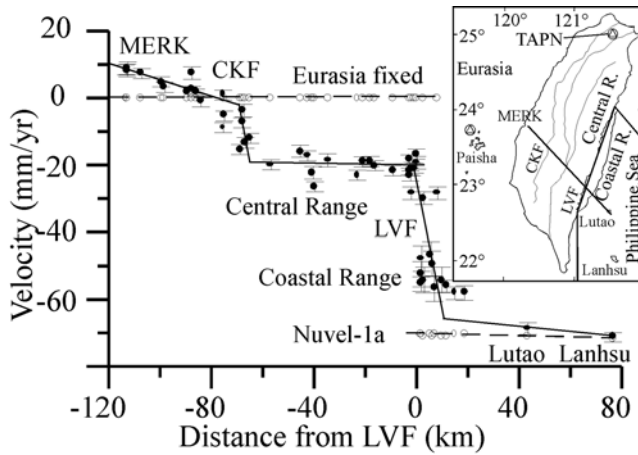


Figure 3. Comparison of GPS velocities in Taiwan area with Nuvel-1A predictions. The GPS data (from Yu *et al.* [1997]) are adapted to the Eurasia-fixed reference frame, projected onto the MERK-Lutao profile (see inset) for all sites within an 82-km wide swath. Negative value represent northwestward velocity component parallel to the profile. The dashed lines are Nuvel-1A velocities for the Philippine Plate with respect to fixed Eurasia. LVF: the Longitude Valley Fault; CKF: the ChuKou Fault.

boundary, the GPS velocity changes sharply. At the Coastal Range the GPS velocity differs nearly 16 mm yr^{-1} from the Nuvel-1A predictions, indicating shortening within the Philippine Sea plate at a strain rate of $\sim 6 \times 10^{-15} \text{ s}^{-1}$, much larger than that across the Himalayan front. The active plate boundary at the LVF is marked by a sharp change (over 30 mm yr^{-1}) of the GPS velocities. However, deformation in the plate boundary zone is complicated and diffuse. Little deformation occurs within the Central Range, as indicated by the uniform GPS velocities, whereas about 20 mm yr^{-1} velocity changes over the Chu-Kou Fault (CKF). To the west of CKF, the GPS velocity changes gradually, indicating a broad zone of crustal shortening in the Western Foothills and the Coast Plain.

3. Discussion

[9] The diffuse plate-boundary deformation and significant intraplate deformation in the three pairs of convergent plates deviate from the paradigm of the plate tectonics theory. However, the plate tectonics theory is based on geological records spanning over millions of years, whereas the GPS data were collected over a period of several years. The relationship between transient strain and permanent deformation across convergent plates can be illustrated using a simple mechanical model (Figures 4a–b). This model provides a first-order approximation of the mechanical behavior of convergent plates: permanent crustal shortening (viscous flow in the dashpot) in collisional boundary zone, elastic deformation within the plates (springs), and plastic slipping (sliding along subduction zone) when tectonic stresses reach the yield strength of the crust. When the system is compressed from the left end of the model at a constant velocity V_0 with respect to the fixed right side, the stress $\sigma(t)$ increases with time: $\sigma(t) = \sigma_b + (V_0\eta/d - \sigma_b)[1 - \exp(-(d/\eta)(L_1/E_1 + L_2/E_2)t)]$, where σ_b is the background stress, t is time, d and η are the width and viscosity of boundary zone, L_1 , E_1 , L_2 , and E_2 are the length and elastic moduli of plates 1 and 2, respectively. Assuming the viscous dashpot is stronger than the sliding plates, i.e., the maximum viscous stress $V_0\eta/d > \sigma_y$, which is the yield strength of the sliding plates, then whenever the stress in the system reaches σ_y , sliding occurs between the frictional plates, the stress drops to σ_b , and the process then repeats.

The corresponding displacements are shown in Figure 4c. The displacement of plate 2 near the boundary zone, U_2 , increases at the velocity V_2 when stress is accumulating but drops to zero when a sliding event occurs. The displacement of plate 1 near the boundary zone, U_1 , increases at the velocity V_1 but jumps up each time when a slip occurs at the plate boundary. The long-term averaged U_1 would approach V_0t . In other words, the long-term averaged GPS velocity would approach that of the rigid-plate

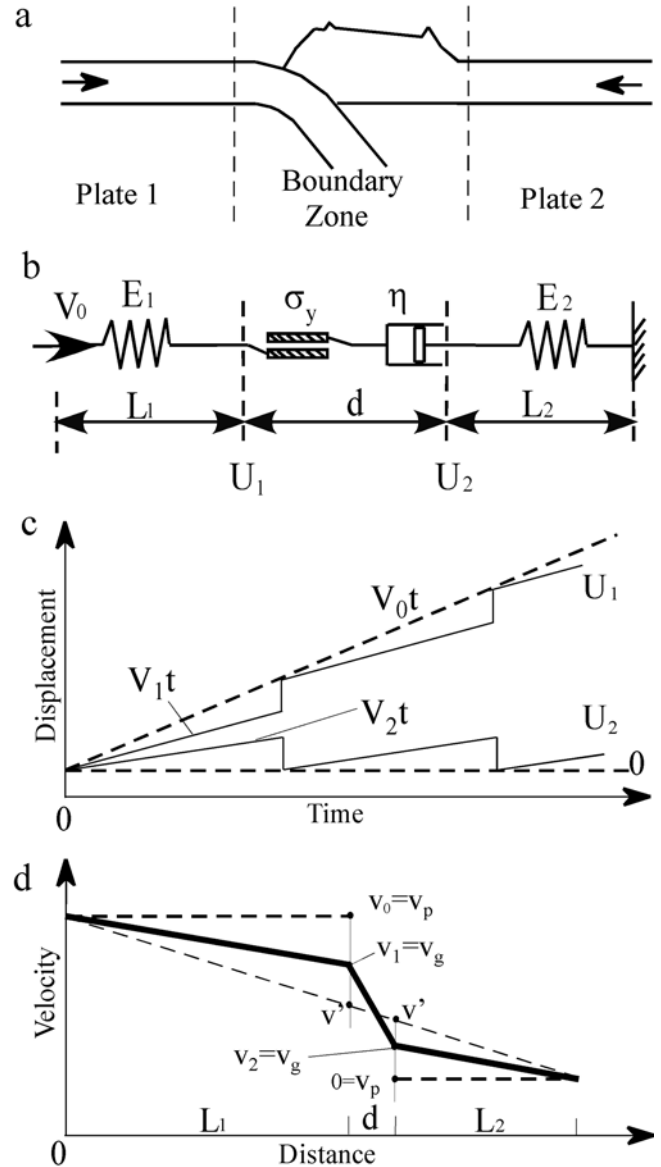


Figure 4. A mechanical model for the deformation of a pair of convergent plates. (a) Sketch of the convergent plates. (b) The mechanic model: springs represent tectonic plates, sliding at the plate boundary are represented by the frictional plates, and permanent deformation at the boundary zone is represented by viscous flow in the dashpot. Convergence of the plates is simulated by fixing the right end and moving the left end at velocity V_0 . (c) Solid lines show the predicted displacements of plates 1 (U_1) and 2 (U_2) near the boundary zone. Dashed line shows the rigid-plate model predictions. (d) The velocity profiles for the mechanical model (thick solid lines), the rigid-plate model (thick dashed lines), and the extreme case when the two plates have identical rheology and are completely coupled (thin dashed lines).

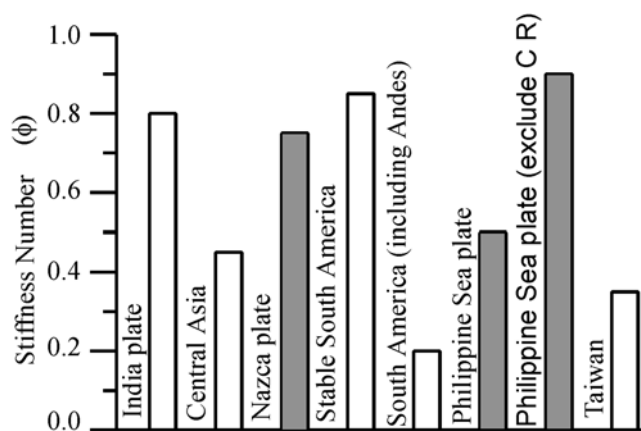


Figure 5. Stiffness number (ϕ) of the plates in this study. Solid bars are oceanic (or part of oceanic) plates. Empty bars are continental (or part of continental) plates. CR: Coastal Range.

motion models. V_1 and V_2 are the instantaneous velocities of the two plates near the boundary zone that would be reflected in GPS measurements. For this model their values depends on the convergence rate and the rheology of the plates: $V_1 = V_0 - kL_1/E_1$ and $V_2 = kL_2/E_2$, where $k \approx (V_0 - \sigma_b d/\eta)/(L_1/E_1 + L_2/E_2)$ when $t < \eta/\text{Max}(E_1, E_2)$.

[10] The instantaneous velocity profile of the model (Figure 4d) is consistent with the GPS velocities across the convergent plate boundaries (see Figures 1–3). The deviation of the GPS velocities from those of plate-motion models depends on the rheology of the convergent plates and the degree of mechanical coupling between the plates. To quantify the non-rigid behavior of the plates we define a stiffness number, ϕ : $\phi = (V' - V_g)/(V' - V_p)$, where V_g is the instantaneous or the GPS velocity near the plate boundary zone, V_p is the velocity at the same location predicted by plate-motion models, and V' is the velocity we would have at the same location if the plates are completely coupled so that there is no plate boundary (see Figure 4d). For this model $V' = V_0(L_2 + d)/L$ for plate 1 and $V' = V_0L_2/L$ for plate 2, here $L = L_1 + d + L_2$. When $V_g = V_p$, $\phi = 1$ and the plate behaves as the perfect rigid plate assumed in classical plate tectonic theory. To the other end, $V_g = V'$ and $\phi = 0$ when the two plates have identical rheology and are completely coupled, so the only strain is intraplate. For convergent plates ϕ provides a measure of their stiffness, or their “plate-like” behavior. Figure 5 shows the ϕ values of the plates in this study. As expected, the oceanic plates have high ϕ values, whereas the central Asia and Taiwan have low ϕ values. Note that stable South America and the India plate are stiffer than the oceanic Nazca plate.

[11] The ϕ value also provides a direct measure of intraplate strain rate relative to the total strain rate across the convergent plates. As shown in Figure 4d, the intraplate strain rate of plate 1 is $\dot{\epsilon} = (V_0 - V_g)/L_1$, whereas the theoretical maximum is $\dot{\epsilon}_{\text{max}} = (V_0 - V')/L_1$. By the definition of ϕ we have $\dot{\epsilon}/\dot{\epsilon}_{\text{max}} = 1 - \phi$. Thus $\phi = 0.8$ for the India plate, for instance, means that the intraplate strain rate is about 20% of the total strain rate across the India plate and that the remaining 80% is consumed by plate boundary deformation.

[12] GPS and other space-based geodetic measurements are playing an increasingly important role in tectonic studies. Interpretation of the tectonic significance of GPS data, however, requires a good understanding of the relationship between instantaneous crustal deformation reflected in most GPS data

and the long-term geological records. Results of this study should be useful for studies of plate boundary deformation in other regions.

[13] **Acknowledgments.** We thank Z.-K. Shen for providing unpublished GPS data of central Asia, and Tim Dixon for providing a preprint. We benefited from discussion with Seth Stein, Tim Dixon, and Z.-K. Shen, and constructive criticism by an anonymous GRL referee. This work was supported by NASA grant NAG5-9145 and NSF grant EAR-9805127.

References

- Angermann, D., J. Klotz, and C. Reigber, Space-geodetic estimation of the Nazca-South America Euler vector, *Earth Planet. Sci. Lett.*, *171*, 329–334, 1999.
- Argus, D. F., and R. G. Gordon, No-net-rotation model of current plate velocities incorporating plate motion model NUVEL-1, *Geophys. Res. Lett.*, *18*, 2039–2042, 1991.
- Chen, Z., B. C. Burchfiel, Y. Liu, R. W. King, L. H. Royden, W. Tang, E. Wang, J. Zhao, and X. Zhang, Global positioning system measurements from eastern Tibet and their implications for India/Eurasia intercontinental deformation, *J. Geophys. Res.*, *105*, 16,215–16,227, 2000.
- DeMets, C., R. G. Gordon, D. F. Argus, and S. Stein, Effect of recent revisions to the geomagnetic reversal time scale on estimates of current plate motion, *Geophys. Res. Lett.*, *21*, 2191–2194, 1994.
- Freymueller, J. T., Z. Yang, Q. Wang, R. Bilham, R. Bendick, K. M. Larson, Q. Chen, C. Xu, W. Jiang, and J. Liu, New Kinematic Data from Asia: Implications for Dynamic Models, *Eos Trans. AGU*, *81*, F1226, 2000.
- Isacks, B. L., Uplift of the central Andean plateau and bending of the Bolivian orocline, *J. Geophys. Res.*, *93*, 3211–3231, 1988.
- Larson, K., R. Burgmann, R. Bilham, and J. T. Freymueller, Kinematics of the India-Eurasia collision zone from GPS measurements, *J. Geophys. Res.*, *104*, 1077–1094, 1999.
- Larson, K. M., J. T. Freymueller, and S. Philippsen, Global plate velocities from the Global Positioning System, *J. Geophys. Res.*, *102*, 9961–9981, 1997.
- Leffler, L., S. Stein, A. Mao, T. Dixon, M. Ellis, L. Ocala, and I. S. Sacks, Constraints on the present-day shortening rate across the Central Eastern Andes from GPS measurements, *Geophys. Res. Lett.*, *24*, 1031–1034, 1997.
- Liu, M., Y. Yang, S. Stein, Y. Zhu, and J. Engeln, Crustal shortening in the Andes: Why do GPS rates differ from geological rates?, *Geophys. Res. Lett.*, *27*, 3005–3008, 2000.
- Norabuena, E., L. Leffler-Griffin, A. Mao, T. Dixon, S. Stein, I. S. Sacks, L. Ocala, and M. Ellis, Space geodetic observations of Nazca-South America convergence along the Central Andes, *Science*, *279*, 358–362, 1998.
- Norabuena, E. O., T. H. Dixon, S. Stein, and C. G. A. Harrison, Decelerating Nazca-South America and Nazca-Pacific plate motions, *Geophys. Res. Lett.*, *26*, 3405–3408, 1999.
- Stein, S., Space geodesy and plate motions, in *Space Geodesy and Geodynamics*, edited by D. E. Smith and D. L. Turcotte, pp. 5–20, American Geophysical Union, Washington, D. C., 1993.
- Singh, S. K., M. Ordaz, R. S. Dattatrayam, and H. K. Gupta, A spectral analysis of the 21 May 1997, Jabalpur, India, earthquake (Mw = 5.8) and estimation of ground motion from future earthquakes in the Indian Shield region, *Bull. Seismo. Soc. Am.*, *89*, 1620–1630, 1999.
- Tapponnier, P., and P. Molnar, Active faulting and Cenozoic tectonics of Tien Shan, Mongolia and Baykal regions, *J. Geophys. Res.*, *84*, 3425–3459, 1979.
- Wang, M., Z.-K. Shen, D. Jackson, A. Yin, Y. Li, C. Zhao, D. Dong, and P. Fang, GPS-derived deformation along the northern rim of the Tibetan plateau and southern Tarim basin, *Eos Trans. AGU*, *80*, F1009, 1999.
- Yu, S. B., H. Y. Chen, and L. C. Kuo, Velocity field of GPS stations in the Taiwan area, in *An introduction to active collision in Taiwan*, pp. 41–59, Elsevier, Amsterdam, Netherlands, 1997.